Simultaneous Segregation at Coherent and Semicoherent Heterophase Interfaces

Aniruddha Biswas,[1] Donald J. Siegel,[2] and David N. Seidman[1]

[1]*Department of Materials Science and Engineering, Northwestern University, 2220 Campus Drive, Evanston, Illinois 60208, USA*
[2]*Mechanical Engineering Department, University of Michigan, 2350 Hayward Street, Ann Arbor, Michigan 48109-2125, USA*

(Received 10 January 2010; published 13 August 2010)

By employing a combination of three-dimensional atom-probe tomography and first-principles calculations, significant qualitative and quantitative differences in solute segregation at coherent and semicoherent interfaces bounding a *single* θ' precipitate in an Al-Cu-based alloy are found. Qualitatively, localized segregation is observed at the semicoherent interface, whereas delocalized behavior is present at the coherent facets. Quantitatively, segregation at the semicoherent interface is a factor of 2 greater than at the coherent interface, resulting in a decrease in interfacial energy that is more than 5 times greater than that observed at the coherent facet. These observations illustrate unambiguously the strong couplings among interface structure, chemical composition, and energetics.

DOI: 10.1103/PhysRevLett.105.076102 PACS numbers: 68.35.Dv, 68.35.Md

Precipitation strengthening is widely used for increasing the strength of metallic alloys. For example, in the automobile industry about a billion pounds of precipitation-strengthened Al alloys are used annually in internal combustion engines. Precipitation strengthening involves the addition of alloying elements at concentrations exceeding their solid solubility limits. At low temperatures, the supersaturated solute(s) will precipitate out of solution as second-phase precipitates. Since precipitates impede the motion of matrix dislocations [1], a significant increase in yield strength results.

Precipitation strengthening is strongly impacted by the character of the heterophase interface between the matrix and precipitate [1]. Particularly, the excess Helmholtz free energy σ associated with these interfaces controls the height of the free energy barrier for nucleation and concomitantly the number density of nuclei. Furthermore, a reduction in σ associated with the precipitate size distribution function is the thermodynamic driving force for precipitate coarsening. Finally, the anisotropy in interfacial energy among the facets of a precipitate influences the relative areal fraction of a given facet and therefore a precipitate's morphology.

In the case of multicomponent alloys, the *chemistry* (i.e., chemical composition) of the matrix-precipitate interface has the potential to impact strongly interfacial energies via solute atom segregation [2]. Of particular interest are differences in solute-interface interactions occurring at the distinct $\{hkl\}$ facets of a single precipitate. The facets vary in their orientation relationship, termination, and coherency; therefore, different interfacial compositions may be anticipated, resulting in changes to precipitate morphology and coarsening rates. Unfortunately, given the three-dimensional (3D) nature of these buried interfaces, and the need to resolve chemical concentration gradients over interfacial regions on the subnanometer scale, the linkage between interfacial composition and interface structure is not *a priori* obvious.

Towards a more complete understanding of the couplings among interface structure, chemical composition, and energetics in multicomponent concentrated materials, we report direct evidence for significant qualitative and quantitative differences in solute segregation at coherent (CI) and semicoherent (SCI) interfaces bounding a single θ' precipitate in a multicomponent Al alloy. An atom-probe tomograph with a large area detector (200×200 nm^2) permits us to obtain the requisite large data sets ($>10^7$ atoms) containing multiple precipitates despite the small number densities ($\sim 10^{21}$ m^{-3}) and high aspect ratios ($\sim$30:1) of the precipitates [3]. Additionally, first-principles calculations provide energetic explanations for the observed segregation behavior [4]. Our analyses reveal that segregation phenomena at CI and SCI are distinct: At CI the segregation profile is delocalized, whereas pronounced confined (localized) segregation is observed at SCI. Furthermore, the solute concentration levels resulting

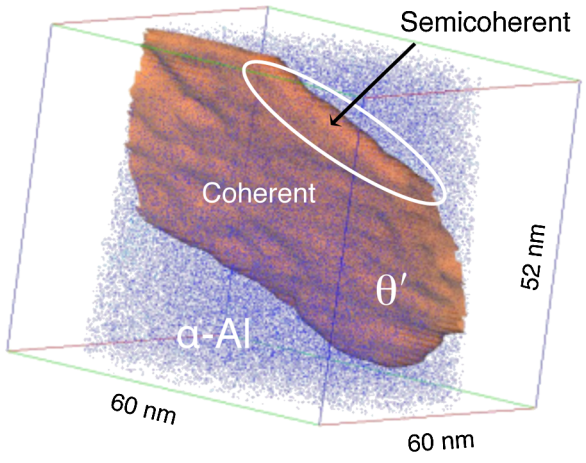

FIG. 1 (color online). 3D LEAP tomographic reconstruction of a θ' precipitate after aging at 463 K for 8 h. A 20 at.% Cu isoconcentration surface delineates the precipitate boundary; for clarity, only Al (blue) and Cu (red) atoms are displayed.

from decreases in the interfacial free energies are different. Segregation at the SCI is a factor of 2 greater than at the CI because its decrease in σ is more than 5 times greater than for the CI. This combination of experiment and computation [5] permits us to verify unambiguously the effects of coherency.

Experiments were performed on a multicomponent Al alloy (7.38 Si-1.54 Cu-0.17 Fe-0.35 Mg-0.13 Mn-0.05 Zn-balance Al, at. %), exhibiting θ' Al_2Cu precipitates [3]. These precipitates possess a platelike morphology with CI to the α-Al matrix along its broad flat faces and SCI at its periphery (Fig. 1) [6]. This morphology is interpretable in terms of a large anisotropy in σ, with the CI possessing a smaller σ (170 mJ m^{-2}) compared to the SCI (520 mJ m^{-2}) (also see Fig. 3) [6,7].

Samples were homogenized in air at 758 K for 24 h, followed by water quenching to 300 K, and then aged in air at 463 K for 8 h or at 533 K for 4 h. Aged samples were characterized by powder diffraction using synchrotron radiation at the Advanced Photon Source (Argonne National Laboratory), and the presence of θ' precipitates was confirmed for both aging conditions. A 3D local-electrode atom-probe (LEAP) tomograph [8,9] was used with a specimen temperature of 40 ± 0.3 K and with a picosecond laser (λ = 532 nm) pulse energy and repetition rate of 0.7 nJ and 500 kHz, respectively. Samples were prepared by using a dual-beam focused ion beam microscope [10]. The proximity histogram method [11] was used for compositional analysis (Fig. 2).

3D LEAP tomography results reveal a thin (~2 nm) and broad (~60 nm) platelet morphology [3] of θ' precipitates (Fig. 1). By amassing large data sets we have imaged and analyzed both CI and SCI between the precipitate and the α-Al matrix. The proxigrams [11] in Fig. 2 compare the concentrations of Al, Cu, Mg, Si, and Zn as a function of distance from the CI (left) and the SCI (right) after aging at 463 K for 8 h. The most striking result is a clear difference in the qualitative nature of segregation between CI and SCI: Significant confined segregation of Si and Mg is localized within ~1 nm of the SCI, whereas the segregation profile at the CI is delocalized (decaying gradually into the precipitate core) and exhibits smaller peak solute concentrations. Significant segregation of Zn, Fe, or Mn was not observed. Samples aged at 533 K (not shown) exhibit similar segregation profiles but with smaller peak solute concentrations.

We quantify segregation utilizing the relative Gibbsian interfacial excess Γ_i^{rel}. For a planar interface between a system with two phases, α and β, and $n = 3$ components, Γ_i^{rel} for component i is given by [12]

$$\Gamma_i^{\mathrm{rel}} = \tilde{\Gamma}_i - \tilde{\Gamma}_1 \frac{c_i^\alpha c_2^\beta - c_i^\beta c_2^\alpha}{c_1^\alpha c_2^\beta - c_1^\beta c_2^\alpha} - \tilde{\Gamma}_2 \frac{c_1^\alpha c_i^\beta - c_1^\beta c_i^\alpha}{c_1^\alpha c_2^\beta - c_1^\beta c_2^\alpha}, \quad (1)$$

where the $\tilde{\Gamma}_i$'s are determined by using proxigram concentration profiles: $\tilde{\Gamma}_i = \rho \Delta x \sum_{m=1}^{p} (c_i^m - c_i^k)$. Here ρ is the atomic density, Δx is the distance between the p concentration data points in the proxigram, c_i^k is the concentration of component i at each data point $k = \alpha$ on the α-Al matrix side, and $k = \beta$ on the θ' side of the heterophase interface. A similar method has been used for grain boundaries [13] and at heterophase interfaces in Al-Sc-Mg alloys [14]. At the SCI for samples aged at 463 K, Γ_i^{rel} for Si and Mg with respect to Al and Cu are 10.04 and 4.65 atoms nm^{-2}, respectively (Table I). These values are ~4–6 times greater than that found for the CI. As expected, aging at 533 K reduces the interfacial excesses at both interfaces.

From the Gibbs adsorption theorem, the coefficient of reduction of σ due to segregation of component i with concentration c_i at the interface is given by [13–15]

$$\left.\frac{\partial \sigma}{\partial c_i}\right|_{T,P,\mu_3,\ldots,\mu_{i-1},\mu_{i+1},\ldots,\mu_n} = -k_B T \frac{\Gamma_i^{\mathrm{rel}}}{c_i}, \quad (2)$$

where μ_i is the chemical potential of component i and P is the pressure. For the value of $\Gamma_{\mathrm{Si}}^{\mathrm{rel}}$ measured above (10.04 atoms nm^{-2} for Si at the SCI), we find a value of 17 828 mJ m^{-2} (at.fr.)$^{-1}$ for the corresponding coefficient of reduction of σ. Assuming a linear dependency of σ on solute segregation, the total reduction of the interfacial energy ($\Delta\sigma$) is determined by multiplying the coefficient of reduction by the solute concentration c_i.

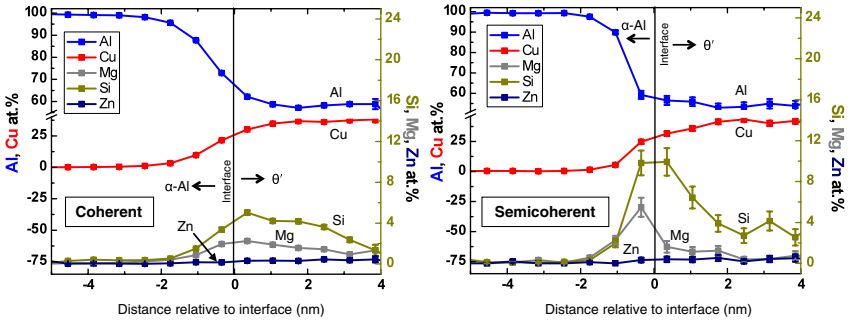

FIG. 2 (color online). Concentrations of Al, Cu, Mg, Si, and Zn as a function of distance from the coherent (left) and semicoherent (right) α-Al/θ' matrix-precipitate interfaces after aging at 463 K for 8 h. Al and Cu levels are identified on the left ordinates; Si, Mg, and Zn levels appear on the right. The location of each interface is depicted with a vertical line; error bars correspond to 2 standard deviations. (Error bars for the CI data are comparable in size to the data symbols.)

TABLE I. Solute concentration (c_i), relative Gibbsian interfacial excess (Γ_i^{rel}), and the change in interfacial energy ($\Delta\sigma$) due to Si and Mg segregation at the coherent and semicoherent matrix-precipitate interfaces as a function of aging condition.

		Semicoherent interface			Coherent interface		
Aging	Solute	c_i (at. %)	Γ_i^{rel} (at./nm^2)	$\Delta\sigma$ (mJ/m^2)	c_i (at. %)	Γ_i^{rel} (at./nm^2)	$\Delta\sigma$ (mJ/m^2)
463 K, 8 h	Si	9.91 ± 1.3	10.04 ± 1.43	-64	5.02 ± 0.2	1.72 ± 0.08	-11
	Mg	5.49 ± 0.9	4.65 ± 1.03	-30	2.25 ± 0.16	1.11 ± 0.08	-7
533 K, 4 h	Si	3.95 ± 0.43	2.94 ± 0.38	-22	1.60 ± 0.19	0.065 ± 0.01	~ 0
	Mg	1.46 ± 0.26	1.62 ± 0.34	-12	0.24 ± 0.07	0.037 ± 0.01	~ 0

Table I summarizes the concentrations of segregated Si and Mg solutes, their relative interfacial excesses, the resultant reductions in σ at both interfaces, and aging conditions. Measured solute concentrations at the SCI are approximately twice those observed at the CI; relative interfacial excesses are also greater by a factor of ~ 4. Significantly, the higher degree of segregation at the SCI results in a reduction in σ that is *5 times greater* than that observed for the CI. These results constitute definitive quantitative and qualitative evidence for the distinct nature of solute segregation at interfaces exhibiting differing states of coherency and, furthermore, illustrate that localized and delocalized segregation can occur at the same precipitate *simultaneously*. In general, the segregation profile at planar defects depends on both the dislocation structure of the interface and on thermodynamics. While it can be difficult to decouple these effects, the fixed composition of the alloy examined here (and hence fixed thermodynamics) suggests that dislocation structure is the predominant factor in determining segregation behavior in this system. In particular, we note that the SCI contain a high density of misfit dislocations (spacing $d \approx 11.6$ Å); these dislocations are absent from the CI. Prior studies of segregation have illustrated the importance of interactions between segregants and dislocation cores [16].

To provide an energetic basis for the measured segregation behavior, the energies at 0 K for Si, Mg, and Zn solute segregation (ΔE_{seg}) at the coherent and semicoherent interfaces were calculated by using density functional theory [17,18]. The two interface supercells employed are illustrated in Fig. 3. Both models adopt the experimental precipitate-matrix orientation relationship $(001)_{\theta'}||\{001\}_{\mathrm{Al}}$ and $[010]_{\theta'}||[010]_{\mathrm{Al}}$ and are based on existing atomistic models [6]. The CI model (Fig. 3, top) exhibits a small misfit strain of 0.7%, whereas the semicoherent model (Fig. 3, bottom) is strained by 5.1%.

Figure 4 plots ΔE_{seg} as a function of position relative to the interface for the CI (left) and SCI (right). (Sites having $\Delta E_{\mathrm{seg}} < 0$ are favorable for segregation.) The far left data points, labeled "Al_b," refer to a bulklike substitutional site in the α-Al matrix; similarly, the far right point "θ'_b" refers to a bulklike site within θ'. The separate data traces within each plot reflect the number of symmetry-distinct segregation sites near the interface planes.

Overall, the calculated segregation behavior is in very good agreement with the rank ordering of solute concentrations observed experimentally: Si > Mg > Zn. Accounting for site competition [19], and counting only sites having moderately strong segregation energies ($\Delta E_{\mathrm{seg}} \leq -0.10$ eV), we find that (across both interfaces) 11 sites are favorable for Si segregation, whereas two are attractive for Mg and only one for Zn. Moreover, the number of favorable segregation sites for all solutes at the SCI (10) is significantly greater than at the CI (4), consistent with the larger solute concentrations measured at the SCI.

Regarding the spatial extent of the solute interfacial concentration profiles (i.e., localized vs delocalized), the distribution of segregation energies in Fig. 4 appears to reproduce approximately the experimental data. For example, compared to the CI, the SCI exhibit favorable ΔE_{seg} values that are more strongly localized near the interface plane. For Si segregation at the SCI, the ΔE_{seg} profile exhibits a minimum at the α-Al interfacial plane (Al_i) and then decays for 3 adjacent layers into the θ' bulk. Like-

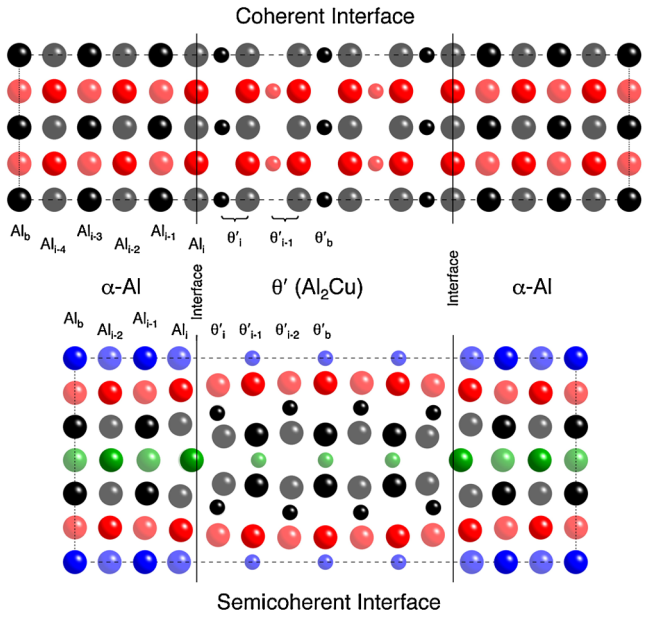

FIG. 3 (color online). Relaxed atomic models for the coherent (top) and semicoherent (bottom) α-Al/θ' interfaces used in our first-principles calculations. Large spheres represent Al atoms, and small spheres represent Cu atoms; atoms are color-coded according to the data traces for ΔE_{seg} shown in Fig. 4. Atomic planes within the Al matrix are labeled as Al_n; planes within θ' are labeled as θ'_n.

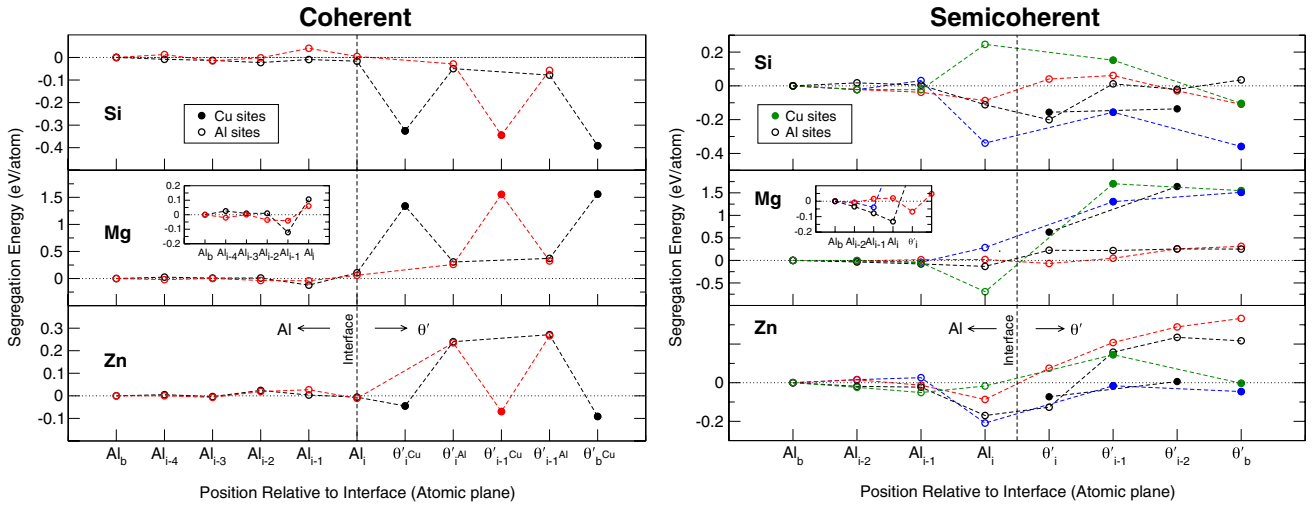

FIG. 4 (color online). Calculated solute segregation energies for Si, Mg, and Zn as a function of distance from the coherent (left) and semicoherent (right) α-Al/θ' interfaces. Segregation at Cu- or Al-sublattice sites in θ' is distinguished by use of filled and open circles, respectively. The inset plots provide a magnified view of the segregation energy of Mg at sites near the interfaces.

wise, the SCI ΔE_{seg} values for Mg display a sharp minimum only at the α-Al interfacial layer, in further agreement with the 3D LEAP data. For the CI, Si segregation is strongly favored at θ' Cu-sublattice sites, and the calculated ΔE_{seg} are nearly independent of depth; such behavior is consistent with the broad Si concentration profile observed experimentally. On the other hand, ΔE_{seg} for Mg, while favorable for the Al_i layer, is positive for layers deeper into θ'. This discrepancy with the 3D LEAP tomographic data may arise from the neglect of shorter-ranged solute-solute interactions in our supercell model, which have been shown to increase segregation at some grain boundaries [20]. Finally, for Zn, our calculations suggest that the negligible segregation observed by LEAP tomographic experiments at both interfaces arises from a combination of relatively small segregation energies and from site competition with stronger-segregating Si and Mg solutes.

In summary, a combination of 3D LEAP tomographic experiments and first-principles calculations have been used to characterize differences in interfacial solute segregation arising from the coherency state of the heterophase interfaces bounding a *single* nanoscale θ' precipitate. Both the magnitude and spatial distributions of the interfacial solute concentrations are strongly coupled to the density of interfacial misfit dislocations, with the semicoherent interface exhibiting significantly larger solute concentrations that are localized near the interface. First-principles calculations suggest that the measured segregation behavior can largely be explained by the energetics of noninteracting solute atoms. Our findings provide clear evidence of the intimate couplings among interface structure, chemical composition, and energetics.

We acknowledge the Ford-Boeing-Northwestern Alliance for financial support and thank J. Allison, M. Li, D. Shih, M. Krug, and C. Wolverton for helpful suggestions. Funds for the LEAP were provided by ONR DURIP and NSF MRI.

[1] J.-L. Strudel, in *Physical Metallurgy*, edited by R. W. Cahn and P. Haasen (North-Holland, Amsterdam, 1983), Vol. 2.
[2] A. P. Sutton and R. W. Balluffi, *Interfaces in Crystalline Materials* (Oxford University Press, Oxford, 1995).
[3] S. C. Weakley-Bolin, W. Donlon, C. Wolverton, J. W. Jones, and J. E. Allison, Metall. Mater. Trans. A **35**, 2407 (2004).
[4] Y. Mishin, M. Asta, and J. Li, Acta Mater. **58**, 1117 (2010).
[5] D. N. Seidman, Annu. Rev. Mater. Res. **32**, 235 (2002).
[6] V. Vaithyanathan, C. Wolverton, and L. Q. Chen, Acta Mater. **52**, 2973 (2004).
[7] E. A. Marquis and D. N. Seidman, Acta Mater. **49**, 1909 (2001).
[8] T. F. Kelly *et al.*, Annu. Rev. Mater. Res. **37**, 681 (2007).
[9] D. N. Seidman, Annu. Rev. Mater. Res. **37**, 127 (2007).
[10] K. Thompson *et al.*, Ultramicroscopy **107**, 131 (2007).
[11] O. C. Hellman, J. A. Vandenbroucke, J. Rusing, D. Isheim, and D. N. Seidman, Microsc. Microanal. **6**, 437 (2000).
[12] S. A. Dregia and P. Wynblatt, Acta Metall. Mater. **39**, 771 (1991).
[13] B. W. Krakauer and D. N. Seidman, Acta Mater. **46**, 6145 (1998).
[14] E. A. Marquis *et al.*, Phys. Rev. Lett. **91**, 036101 (2003).
[15] E. A. Marquis, D. N. Seidman, M. Asta, and C. Woodward, Acta Mater. **54**, 119 (2006).
[16] J. D. Rittner and D. N. Seidman, Acta Mater. **45**, 3191 (1997).
[17] G. Kresse and J. Furthmüller, Phys. Rev. B **54**, 11 169 (1996).
[18] J. P. Perdew *et al.*, Phys. Rev. B **46**, 6671 (1992).
[19] A site will be occupied by the solute having the most favorable ΔE_{seg}.
[20] D. J. Siegel and J. C. Hamilton, Acta Mater. **53**, 87 (2005).